

**DETAILED GEOMORPHOLOGIC ANALYSIS OF LUNAR REGIONS OF INTERESTS.** M. L. Meier<sup>1</sup>, K. R. Frizzell<sup>2</sup>, G. R. L. Kodikara<sup>3</sup>, M. A. Kopp<sup>4</sup>, K. M. Luchsinger<sup>5</sup>, A. Madera<sup>6</sup>, T. G. Paladino<sup>7</sup>, C. J. Tai Udovicic<sup>8</sup>, R. V. Patterson<sup>9</sup>, and D. A. Kring<sup>10</sup>, <sup>1</sup>University of Florida (mckaylameier@ufl.edu), <sup>2</sup>Arizona State University, <sup>3</sup>University of Wisconsin – Milwaukee, <sup>4</sup>Boston College, <sup>5</sup>NASA Ames, <sup>6</sup>Rutgers University, <sup>7</sup>Idaho State University, <sup>8</sup>University of Hawaii, <sup>9</sup>University of Houston, <sup>10</sup>Lunar and Planetary Institute.

**Introduction:** In support of the upcoming crewed and uncrewed Artemis missions [1] to the lunar south polar region, we assess morphological parameters, trafficability, and sampling opportunities associated with three regions of interests (ROIs).

*Geologic Context.* The lunar south polar region hosts a variety of rock and potentially ice compositions that address key questions pertaining to lunar formation, differentiation history, and impact processes (e.g., [2-8]). Previous infrared spectroscopy studies reflect the lunar south polar region as predominantly feldspathic terrain reworked through heavy cratering processes, with ages ranging from 3.5 to 4.5 Ga [6, 9-12]. The region may contain crystalline anorthositic, mafic, ultramafic, basaltic, and impact-derived melt rocks and breccias composed of them [2]. Lithologies may provide clues about lunar magma ocean processes [13], including mantle compositions and overturn [7], and the consequences of the SPA impact, circa 4.25 to 4.35 Ga [14-16]. We identify locations optimal for diverse geologic sampling correlating to trafficability.

**Study Regions:** We present one selected (Site 102) and two potential (Site 105 and Upper Right Quadrant of Shackleton crater) regions assessed for geomorphology, resources, and hazards (Figure 1). Our study regions are representative of previously selected ROIs and build upon prior analysis of other ROIs [17].  
*Site 102.* As a selected study region for the NASA VIPER (Volatiles Investigating Polar Exploration Rover) mission planned for late 2025, we investigate Site 102 (85.43° S, 31.73° E) near Nobile Crater [18-19]. Site 102 is positioned on near the western edge of Nobile crater, on Mons Mouton [18-19]. Mons Mouton averages illumination over 50% annually and has direct line-of-sight to Earth (as located on the nearside) as one of the highest elevation summit in the south polar region. The massif is heavily cratered with locations capable of hosting permanently shadowed regions (PSRs), traps for water- and dry-ice deposits, (e.g. [20-21]) and therefore a prime locations for *in situ* resource utilization (ISRU). Along with high potential for ISRU, Mons Mouton massif is the product of dynamic and diverse geologic processes. The massif was uplifted during the SPA impact event, exposing Pre-Nectarian aged deposits in a vertical cross-section of the upper crust. Additionally, the range may have been blanketed with SPA ejecta composed of upper mantle

and lower crustal material of the lunar farside [7,22]. As cratering continued, Mons Mouton is likely to have ejecta deposited from nearby younger craters, including that of Nobile crater (3.8 Ga [9]). This sequence of events likely produced and preserved deposits of diverse lunar ices with ISRU potential along with a lithologic units that can better constrain lunar chronology

*Site 105.* Site 105 (87.18° S, 62.83° E) is a shallowly sloped (<15°) ridgeline between Faustini (4.10 Ga [6]) and Shoemaker (4.15 Ga [6,17,23]) craters [23-24]. This interplain region is likely rich in geologic diversity as Shoemaker and Faustini impacts deposited Nectarian ejecta over a prominent Pre-Nectarian Terra crustal layer [2,10]. These layers have likely been partially reworked through impact gardening [25], along with the potential for boulder deposits from VIPER landing site due to the high degree of slope between the locations [26]. The significant cratering of the ridgeline reflects large PSR coverage within the craters, and thus potential for ice retention and ISRU.

*Upper Right Quadrant of Shackleton Crater.* As an Imbrium-aged crater, Shackleton forms the edge of the SPA basin and the center of the lunar south pole [2,6,17]. Shackleton Crater (89.32° S, 75.30° E) and the surrounding regions have been of interest for landing site and base camp potential due to the abundant geologic diversity and access to ROIs [27]. The interplain region between Shackleton and Shoemaker craters reflects many rock outcrops and boulders, with the high potential for geologic sampling.

**Data Acquisition and Analysis:** Our study reflects analysis of the morphology, sampling interests, and trafficability of our sites in ArcGIS Pro. We investigate terrain within 2, 10, and 20 km radial exploration zones suitable for rover and human exploration distances anticipated for Artemis missions.

*Geomorphic Parameters.* Digital elevation models (5 km/pixel and 30 km/pixel resolution) [28] are utilized to produce hillshade, topographic, and slope maps of the three sites. In combination with high resolution (0.5-1 m resolution) Narrow Angle Camera imagery (from NASA MoonTrek Mosaic and the Planetary Data System), we produce geomorphic maps with differentiation of subunits based on slope degrees.

*Sample Selection.* For sampling selection, we address two methods pertaining to sampling of rock or ice. For rock sampling, we identify different outcrop

features using the geomorphic datasets, including rock outcrops, boulders, boulder fields, and scarps.

For lunar ices, we identify PSR locations via temperature, creating maps of potential seasonal water and dry-ice thermal stability. PSR and illumination [29] were mapped (120 m resolution) in comparison to maximum seasonal bolometric temperatures (240 m/pixel resolution) [30] and spectrally identified hydrogen abundance (0.5° by 0.5°/pixel bin) [31]. Areas of potential water- and dry-ice are identified based on modeled maximum ice stability temperatures below 110 K and 55 K [32].

**Trafficability Analysis.** Surface roughness index maps of each of the sites are created using python GDAL wrapper on DEMs [28]. In addition, we account for crater density of terrains to delineate potential traversal pathways.

**Results:** The three sites evaluated in this study reflect geomorphologies in cratering, plains, and ridge units, which are categorized based on location and slope. All sites expose a variety of lithologies with numerous identified potential sampling locations. In contrast to potential rock sampling, ice sampling is significantly more limited. Site 102 potentially retains water-ice in the PSRs formed within a broad secondary crater chain, with traversability to the PSRs. Site 105 reflect cooler temperatures within a 20 km radial zone (with possible water- and dry-ice deposits), spanning potential for lunar ices over a predominantly trafficable area. The interplain region between Shackleton and Shoemaker craters reflects small probable abundances of water-ice within a secondary crater but maintains significant limited trafficability due to the dynamic topography. Overall, we take multi-data approach to address the site selection for the Artemis missions.

**References:** [1] NASA (2020) *Artemis Plan: NASA's Lunar Exploration Program Overview*. [2] Patterson R. V. et al. (2023) *LPS LIII*, Abstract #2806. [3] Borg L. E. et al. (2022) *Proc. Natl. Acad. Sci. U.S.A.*, 119. [4] Kraetli G. et al. (2022) *Icarus*, 371, 114699. [5] Kring D. A. et al. (2021) *Adv. in Space Res.*, 68, 4691–4701. [6] Tye A. R. et al. (2015) *Icarus*, 255, 70–77. [7] Hurwitz D. M.

and Kring D. A. (2014) *JGR Planets*, 119, 1110–1133. [8] Elkins-Tanton L. T. et al. (2011) *Earth and Planet. Sci. Lett.*, 304, 326–336. [9] Deutsch A. N. et al. (2020) *Icarus*, 336, 113455. [10] Spudis P. D. et al. (2008) *GRL*, 35, L14201. [11] Haruyama J. et al. (2008) *Earth, Planets and Space*, 60, 243–255. [12] Stöffler D. et al. (1980) *Proc. Conf. Lunar Highlands Crust*, 51-70. [13] Wood J. A. (1970) *Apollo 11 Lunar Sci. Conf.*, 1, 965-988. [14] Hiesinger H. et al. (2012) *LPS XLIII*, Abstract #2863. [15] Kring D. A. et al. (2015) *Early Solar System Impact Bombardment III*, Abstract #3009. [16] Garrick-Bethell I. et al. (2020) *Icarus*, 338, 113430. [17] Gawronska A.J. et al. (2020) *Advances in Space Research*, 66, 1247-1264. [18] Colaprete A. et al. (2020) *LPS LI*, Abstract #2241 [19] NASA (2021) *Volatiles Investigating Polar Exploration Rover Proposal Information Package*. [20] Kring D. A. et al. (2020) *LPS LI*, Abstract #1933. [21] Lemelin M. et al. (2021) *PSJ*, 2, 103. [22] Potter R. W. et al. (2012) *Icarus*, 220, 730–743. [23] Flahaut J. et al. (2020) *Planet. Space Sci.* 180, 104750. [24] Mazarico E. et al. (2011) *Icarus*, 211(2), 10661081. [25] Costello E. S. et al. (2021) *JGR Planets*, 126. [26] Kring D. A. and Durda D. (2012) *LPI*, Contr. #1694, pp. 688. [27] Kring D. A. et al. (2023) *IEEE Aerospace Conf.*, 1-17. [28] Barker M. K. et al. (2021) *Planetary & Space Science*, 203, 105119. [29] Mazarico et al. (2017) *Icarus*, 211- 2, 1066-1081. [30] Williams J.P. et al. (2019) *JGR Planets*, 124, 25052521. [31] Feldman W.C. et al. (2001) *JGR Planets*, 106, 23231-23251. [32] Zhang J.A. and Paige D.A. (2009) *GRL*, 36.

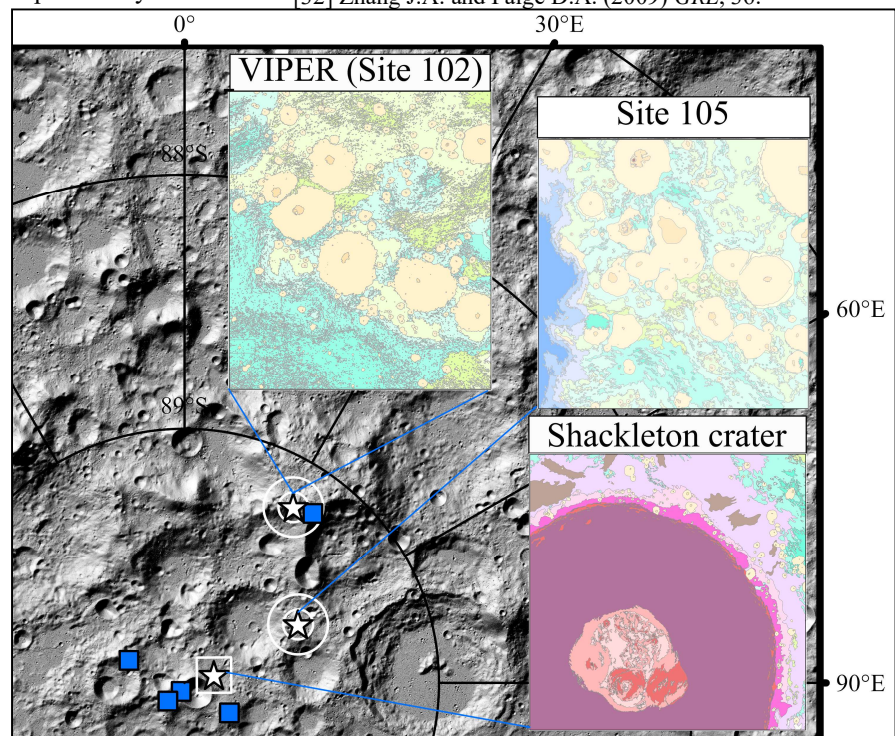


Figure 1. Geomorphic analysis maps of Site 102, Site 105, and Shackleton crater. Basemap features 30 m/pixel resolution hillshade of the lunar south polar region with ROIs in blue squares, with the three sites of our study represented by stars. The geomorphic maps represent units of ridges (blue/green), plains (light green), craters (tans/yellows), and location-specific units for Shackleton (reds/pinks) and Shoemaker (deep blues) craters. Each of the major units (craters, plains, and ridges) are differentiated by high (>20°), moderate (10-20°) and low (<10°) slopes, with deeper colors reflecting higher slopes.